Available online at www.sciencedirect.com
ScienceDirect
Solar Energy 81 (2007) 977–992
SOLAR ENERGY
www.elsevier.com/locate/solener

Development of a suitable model for characterizing photovoltaic arrays with shaded solar cells

Engin Karatepe *, Mutlu Boztepe, Metin Çolak

Department of Electrical and Electronics Engineering, Engineering Faculty, Ege University, 35100 Bornova-Izmir, Turkey

Received 28 September 2005; received in revised form 12 May 2006; accepted 12 December 2006
Available online 17 January 2007

Communicated by: Associate Editor Aaron Sanchez-Juarez

Abstract

The aim of this study is to investigate the effects of non-uniform solar irradiation distribution on energy output of different interconnected configurations in photovoltaic (PV) arrays. In order to find which configuration is less susceptible to mismatch effects, a PV module model is developed. This model can take into consideration the effects of bypass diodes and the variation of the equivalent circuit parameters with respect to operating conditions. The proposed model can provide sufficient degree of precision as well as solar cell-based analysis in analyzing large scale PV arrays without increasing the computational effort. In order to produce more reliable and robust simulations, improved and extended algorithms are presented. Some results are discussed in detail and some recommendations are extracted by testing several shading scenarios.

Keywords: Photovoltaic arrays; Equivalent circuit parameters; Shading; Mismatching

1. Introduction

The increasing world's energy demands and environmental pollution are motivating research and technological investments related to improved energy efficiency and generation. In practical applications, a PV module consists of 36 solar cells which are connected in series and PV modules are wired together into array both in series and in parallel to provide the necessary voltage and/or currents. The output power of a PV array decreases considerably, when current–voltage (I–V) curves of solar cells are not identical due to soiling, non-uniform irradiation and temperature variations, cell damaging, partially, shading etc. (Oozeki et al., 2003; Kawamura et al., 2003; Dyk et al., 2002; Meyer and Dyk, 2004; Weinstock and Appelbaum, 2004). These are the main reasons of mismatch. In recent years, the impact of partial shadowing on the energy yield of PV systems has been widely discussed (Woyte et al., 2003; Quaschning and Hanitsch, 1996; Kaushika and Gautam, 2003; Ho and Wenham, 2001). Before trying to eliminate or reduce mismatch effects, a thorough understanding of their origin and behavior is required. Since the field testing is costly, time consuming and depends heavily on the prevailing weather condition, it is necessary to define a circuit based simulation model which properly allows the inclusion of mismatch effects with high accuracy.

The equivalent circuit generally used for PV module or solar cell is shown in Fig. 1 (Duffie and Beckman, 1991). The relationship between solar cell's current and voltage has both the implicit and nonlinear mathematical equations. Therefore, determination of the equivalent circuit parameters requires more computational effort for each operating condition when electrical performance is analyzed (Teng and Wu, 1989; Araki and Yamaguchi, 2003; Merten et al., 1998; Ikegami et al., 2001). In most studies, only the photo-current and the diode saturation current

* Corresponding author. Tel.: +90 232 3434000/5243; fax: +90 232 3886024.
E-mail address: engin.karatepe@ege.edu.tr (E. Karatepe).

0038-092X/$ - see front matter © 2006 Elsevier Ltd. All rights reserved.
doi:10.1016/j.solener.2006.12.001

Nomenclature

c	number of total solar cells in a single PV module	R_s^{cell}	series resistance of solar cell (Ω)
d	number of bypass diodes in a single PV module	R_p^{cell}	parallel resistance of solar cell (Ω)
I	current (A)	s	number of PV module in a column of PV array
I_{ph}	photo-current (A)	T	temperature
I_s	diode saturation current (A)	T_{bd}	bypass diode temperature
I_{sbd}	saturation current of bypass diode (A)	V	voltage (V)
I_{sc}	short circuit current (A)	V_{mp}	voltage at maximum power point
k	Boltzman constant (J/K)	V_{load}	load voltage at output of PV array (V)
n	diode ideality factor of solar cell	V_{oc}	open circuit voltage (V)
n_{bd}	ideality factor of bypass diode		
N_s	number of solar cells in series for a single PV module	*Index*	
		MPP	maximum power point
p	number of solar cells per a single bypass diode	TCT	total cross tied configuration
q	electric charge (C)	BL	bridge link configuration
r	number of PV module in a row of PV array	SP	series–parallel configuration
R_s	series resistance of PV module (Ω)	ANN	artificial neural network
R_p	parallel resistance of PV module (Ω)	RMSD	root mean square deviation

are changed with irradiation and temperature, respectively, and the other parameters are determined by taking a reference operating condition (Quaschning and Hanitsch, 1996; Kaushika and Gautam, 2003; Duffie and Beckman, 1991; Ikegami et al., 2001). However, all of the circuit parameters depend on both irradiation and cell temperature and the relationship between them is nonlinear and cannot be easily expressed by an analytical equation (Blas et al., 2002; Lu and Yang, 2004; Gow and Manning, 1999; El-Adawi and Al-Nuaim, 2002; Sharma et al., 1991). In addition, some differences can be seen in the equations that describe the relationship between the parameters and operational conditions (Lu and Yang, 2004; Gow and Manning, 1999). So, every assumption forces the model to fall into error. For this reason an assumption should be done carefully, especially in simulation studies of PV arrays under mismatch conditions and low irradiated PV modules (Karatepe et al., 2006). Sharma et al. (1991) showed that consideration of identical series and parallel resistances for illuminated and dark region of a PV module is not a valid assumption and enhancement of the resistances must be considered in the analysis of partially shaded PV array. Dyk and Meyer (2004) also showed that the effects of parallel and series resistances on the PV module performance are significant.

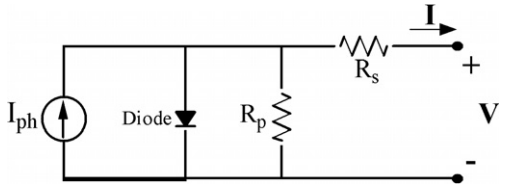

Fig. 1. Solar cell or PV module equivalent circuit.

In this study, firstly, the dependence of all circuit parameters on module temperature and irradiance is included by using artificial neural network (ANN). The advantages of neural-network are used such that there is no requirement of the knowledge of internal system parameters, less computational effort, and a compact solution for multivariable problems.

After improving the accuracy of equivalent circuit of PV module model for all operating conditions, the performance of different interconnected PV arrays are investigated by including bypass diode under different mismatch conditions. In recent years, various series–parallel combinations of PV modules have been proposed to minimize the mismatch effects (Kaushika and Gautam, 2003; Ho and Wenham, 2001). Kaushika and Gautam (2003) did not consider the bypass diode effects and variations in equivalent circuit parameters. In practical applications, PV module incorporates two bypass diodes to prevent the solar cell from non-recoverable reverse bias breakdown and hot-spots, and excessive power depletion as a result of mismatch effects. The bypass diodes affect the I–V curve of PV array significantly and cause to create one or more local maximum power point (MPP), when an influential mismatch occurs. Therefore, distortion of shaded I–V curve may lead to error in determination of global MPP. Consequently, it is crucial to include bypass diodes for analyzing the I–V characteristics of a PV array (Kawamura et al., 2003; Quaschning and Hanitsch, 1996). The value of parallel resistance is also important for the I–V characteristic because of the electrical circuit interactions. This effect cannot be seen properly when the identical equivalent circuit parameters set is used for all operating conditions or the series and parallel resistances are ignored. So the I–V characteristic of PV array is fallible if bypass diodes and the resistances are not included.

Another important issue is that shading effects on the performance of PV array are highly dependent upon the direction or shape of the shadow. For this reason, solar cell-based analysis becomes more important than module-based analysis. On the other hand, while simulating the behavior of a large-scale PV array with down to solar cell level, one obvious drawback is the necessity of long computation time (Woyte et al., 2003). In most studies, a PV module that consists of several series connected solar cells is lumped together as a single solar cell for simplicity. Therefore, one of the aims of this study is to present an analysis method to reflect the mismatch effects as well as solar cell-based analysis without increasing computational time, in a simple manner and with sufficient degree of precision. Since there are various possible mismatch scenarios, it is difficult to examine the behavior of PV array for all cases. On the other hand, selecting shading scenario is an important issue especially in configurations that were investigated by Kaushika and Gautam (2003). Some shadow options may give a similar effect for different configurations or one configuration has a better performance for only a specific shading scenario. These factors could lead to an error for finding which configuration has better tolerance due to the shadow problem. Thus, in this study, several inhomogeneous irradiation distributions are used to investigate the behavior of PV arrays. In conclusion, in order to produce more reliable and robust simulations, improved and extended algorithms are presented to evaluate mismatch effects in PV arrays and some results are discussed in detail.

2. Development of PV module model

The one diode equivalent circuit of a solar cell consists of a diode, a current source, a series resistance, and a parallel resistance (Duffie and Beckman, 1991; Teng and Wu, 1989; Araki and Yamaguchi, 2003; Merten et al., 1998; Ikegami et al., 2001). The current source generates photo-current (I_{ph}) which is a function of incident solar irradiation and cell temperature. The diode represents p–n junction of the solar cell. At real solar cells, the voltage loss on the way to the external contacts is observed. This voltage loss is expressed by a series resistance (R_s). Furthermore, leakage currents are described by a parallel resistance (R_p). Using Kirchhoff's first law, the equation for the extended I–V curve is derived as follows:

$$I = I_{ph} - I_s\left(\exp\left(\frac{q(V+IR_s)}{nN_skT}\right) - 1\right) - \frac{V+IR_s}{R_p} \quad (1)$$

where I is the output current of PV module, N_s is the number of solar cells in series for a module, V is the terminal voltage of module, q is the electric charge (1.6×10^{-19} C), k is the Boltzman constant (1.38×10^{-23} J/K), and T is the cell temperature (K). In conventional approach, to decrease the complexity, it is assumed that only photo-current and diode saturation current depend on operational conditions and the others are identical for all conditions (Duffie and Beckman, 1991; Ikegami et al., 2001).

To characterize a PV module as a power source in performance analysis, it is very important to take into consideration the dependence of all equivalent circuit parameters of PV module on irradiation and cell temperature. The five equivalent circuit parameters can be determined by using the available operating points on the I–V curve. To be able to obtain the changing of the parameters over the whole range of operating conditions, Sandia's PV module electrical performance model (King, 2000) is used for generating the required five points on the I–V curve. These points are shown in Fig. 2 for a one operating condition. These points are generated for 209 operating conditions between 15–65 °C and 100–1000 W/m^2 to solve the five coupled implicit nonlinear equations for Siemens SM 55 PV module that consists of 36 series connected monocrystalline silicon solar cells. Table 1 shows the specification of the SM 55 PV module. To solve the nonlinear implicit system of equations, each nonlinear algebraic equation must be written in the form $F(x) = 0$, an expression that is to have the value of zero at the solution. We have five equations and five unknowns for each operating condition and we have to find $x \in \Re^5$. The appropriate form for these equations is

$$F_i = -I_i + x_1 - x_2(\exp(q(V_i + I_i x_4)/x_3 N_s kT) - 1) - (V_i + I_i x_4)/x_5 \quad (2)$$

The trust region optimization method (McCartin, 1998) is used for solving the system of equations. In general, trust-region methods are faster than gradient methods and guarantee the stability regardless of initial conditions.

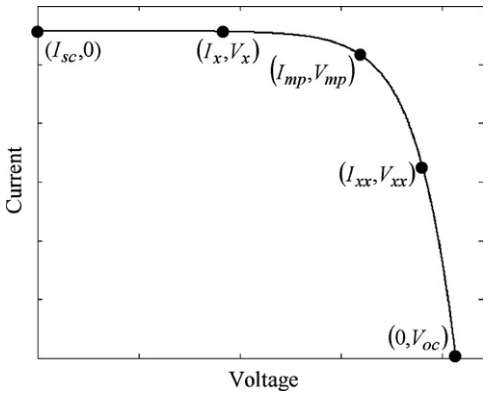

Fig. 2. The used five operating points on the I–V curve of PV module to solve the nonlinear implicit I–V equation for a single operating condition.

Table 1
Specification of SM 55 PV module

Maximum power (P_{mp})	55 W
Open circuit voltage (V_{oc})	21.7 V
Short circuit current (I_{sc})	3.45 A
Operating voltage at maximum power (V_{mp})	17.4 V
Operating current at maximum power (I_{mp})	3.15 A
(AM 1.5, 1000 W/m^2, 25 °C)	

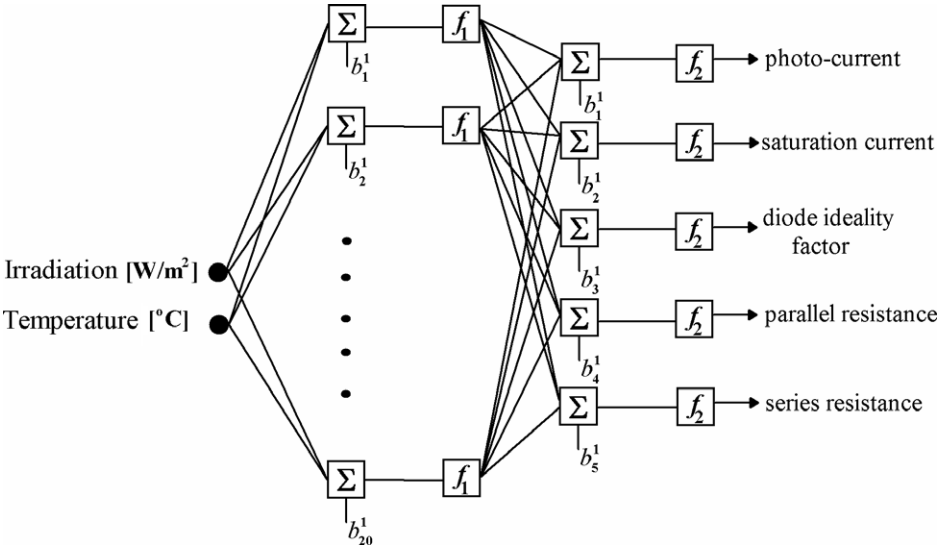

Fig. 3. Configuration of the artificial neural network.

Good initial values are important for solving nonlinear system equations. An initial value that satisfies or closely satisfies many of the constraints reduces the work involved in finding a first feasible solution. At each different operating condition, initial value of the photo-current, series resistance and parallel resistance are estimated by using the corresponding I–V curve. Initial values of the parameters are denoted by the subscript 0 and are given as

$$I_{ph0} = I_{sc} \tag{3}$$

$$R_{s0} = (V_{oc} - V_{xx})/I_{xx} \tag{4}$$

$$R_{p0} = V_x/(I_{sc} - I_x) \tag{5}$$

where I_{sc} is short circuit current, I_x is current at $V_x = 0.5V_{oc}$, I_{xx} is current at $V_{xx} = 0.5(V_{oc} + V_{mp})$, V_{oc} is open circuit voltage, V_{mp} is the voltage at MPP. The more reliable initial values of parallel and series resistances can be obtained by using the short and open circuit slopes of the I–V characteristic (Merten et al., 1998). Initial values of diode ideality factor and saturation current are taken as 1.5 and 10^{-12}, respectively, for all cases.

Obviously, it is quite difficult to determine the parameters for each irradiation and temperature in running simulation studies or on-line PV system applications. For this reason, all parameters are estimated by using ANN. ANN is an alternative way to solve complex problems. In the last decade, significant progresses have been made in ANN technology to expand the range of potential applications in different areas because of the black-box functionality of ANN. The theory of ANN has been described in a large number of published literatures and will not be

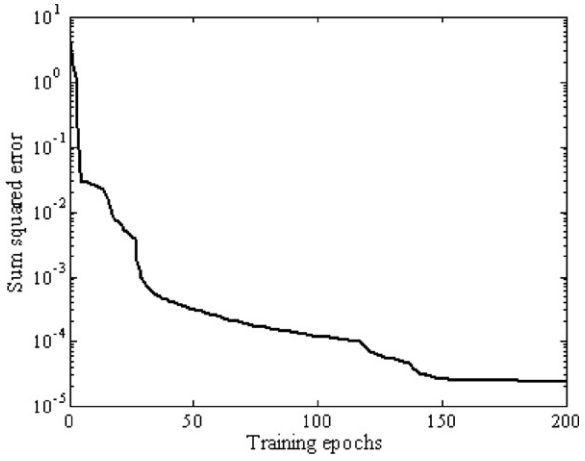

Fig. 4. Representation of the error trend as obtained with the first 200 iterations of the training algorithm of ANN.

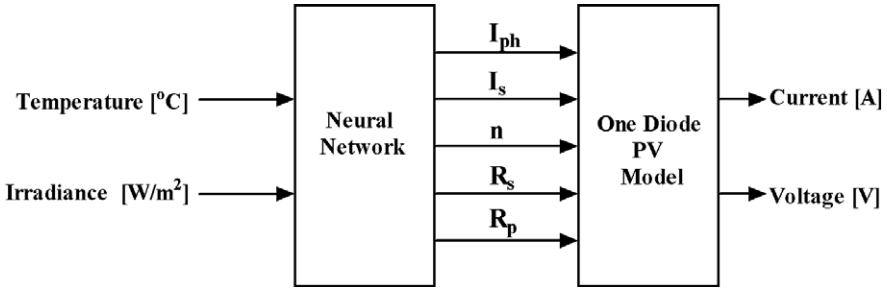

Fig. 5. The basic configuration of the proposed PV model.

Table 2
Estimated equivalent circuit parameters of SM 55 PV module for different operating conditions

Operating conditions	G [W/m^2]	150	350	550	750	950	150	350	550	750	950
	T [°C]	25	25	25	25	25	45	45	45	45	45
PV module equivalent circuit parameters	I_{ph} [A]	0.517	1.207	1.898	2.588	3.278	0.523	1.222	1.920	2.619	3.317
	I_s [μA]	0.007	0.023	0.099	0.346	1.036	0.013	0.033	0.109	0.359	1.019
	n	1.182	1.259	1.362	1.463	1.564	1.039	1.096	1.175	1.261	1.346
	R_s [Ω]	0.831	0.369	0.270	0.223	0.191	1.462	0.631	0.460	0.375	0.323
	R_p [Ω]	2557	1239	875.2	720.7	655.7	1233	591.6	406.1	320.9	275.8
The proposed model	V_{oc} [V]	19.754	20.604	21.057	21.368	21.605	17.890	18.796	19.280	19.612	19.865
	I_{sc} [A]	0.517	1.207	1.897	2.587	3.277	0.523	1.220	1.918	2.615	3.313
	V_{mp} [V]	16.375	17.029	17.251	17.351	17.388	14.484	15.218	15.470	15.548	15.604
	I_{mp} [A]	0.478	1.117	1.749	2.374	2.996	0.476	1.114	1.744	2.373	2.992
	P_{mp} [W]	7.827	19.021	30.172	41.191	52.094	6.894	16.953	26.980	36.895	46.687
SNL model values	V_{oc} [V]	19.794	20.645	21.099	21.411	21.648	17.926	18.834	19.319	19.651	19.905
	I_{sc} [A]	0.517	1.207	1.897	2.587	3.277	0.523	1.220	1.918	2.615	3.313
	V_{mp} [V]	16.381	17.046	17.262	17.355	17.394	14.472	15.224	15.467	15.570	15.614
	I_{mp} [A]	0.480	1.116	1.748	2.374	2.995	0.479	1.115	1.745	2.370	2.990
	P_{mp} [W]	7.863	19.023	30.174	41.201	52.095	6.932	16.975	26.990	36.901	46.686

covered in this paper except for a very brief overview of the used ANN structure.

In this study, to map the relationship between {n, I_s, R_s, R_p, I_{ph}} and {irradiation-module temperature}, the three layer feedforward ANN (input, single hidden, output layer) is used as shown in Fig. 3. The number of nodes in the input and the output layer are based on the input and output dimension, respectively. The number of hidden layer nodes is determined empirically (Reed, 1993). The 20 hidden nodes give the most accurate estimation, therefore only the result of this case is given. Consequently, the input layer has 2 nodes, the hidden layer has 20 nodes, and the output layer has 5 nodes. The input layer in this case consists of a two dimensional vector, irradiation against temperature, and the output vector is five dimensional vector comprising n, I_s, R_s, R_p, and I_{ph}. All data sets are scaled down to the range {−1; 1} and a hyperbolic tangent sigmoid transfer function is used to be the activation function of the single hidden layer (Kalman and Kwasny, 1992). A pure linear function (Zurada, 1992) is chosen as an activation function at the output layer (see Fig. 3).

The learning stage of the network is performed by updating the weights and biases using backpropagation algorithm with Levenberg–Marquardt optimization method (Scales, 1985) in order to minimize the sum of squared differences between the network targets and actual outputs for a given input vector. In order to avoid the network losing the generalization ability, training is stopped when the error on the test set begins to rise considerably (roughly after about 1000 training epochs). Fig. 4 shows the objective function (the sum squared error) evolution after 200 training iterations.

The basic configuration of the proposed PV module model is summarized in Fig. 5. It composes of a two-stage process. Firstly, ANN is used to predict the five parameters by only reading the samples of irradiation and temperature. Secondly, these parameters are put into the one diode electrical equivalent circuit model. The generated data set for 209 operating conditions between 15–65 °C and 100–1000 W/m^2 is subdivided into a training set (199 set) which well describes the entire problem domain, and test sets (10 sets) which are given in Table 2 that also shows the electrical properties and equivalent circuit parameters. The obtained parameters are physically meaningful and match with different models given in the literatures (Blas et al., 2002; Sharma et al., 1991; Virtuani et al., 2003; Ding et al., 2005). Especially the variation of series and parallel resistance with illumination resemble that of the model given in Sharma et al. (1991). Karatepe et al. (2006) showed that it is necessary to properly include the variation of the equivalent circuit parameters in analyzing the I–V characteristics of a PV module, when accurate and reliable performance estimation is required.

3. Solar cell-based simulation model for single PV module

When the part of a PV module is shaded, shaded cells cannot produce as much current as unshaded cells. Since all cells are connected in series in a module, the same amount of current must flow through every cell. Unshaded cells will force shaded cells to pass more current than their new short circuit current. The only way that shaded cells can operate at a current higher than their short circuit current is to operate in the region of negative voltage. This causes a net voltage loss in the system. Shaded cells absorb power and begin to act as a load. In other words, shaded cells dissipate power as heat and cause hot spots. To prevent the hot spot effect, bypass diodes are used in the junction box in PV module. When a solar cell is shaded, the related bypass diode becomes forward biased and all the current greater than the shaded cell's new short circuit current is bypassed through the diode. Thus, bypass diode reduces the amount of local heating drastically at the shaded area. On the other hand, the bypass diode holds

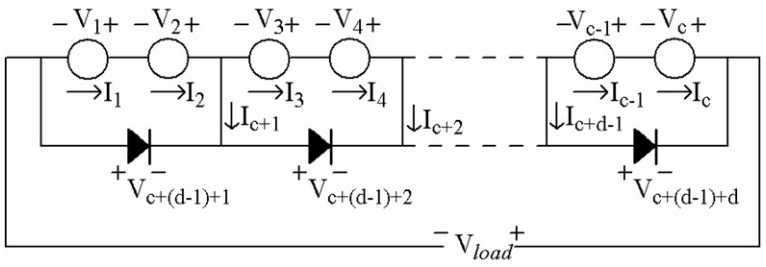

Fig. 6. Solar cell-based single PV module model for the bypass diodes are connected over two solar cells.

the corresponding group of cells to a small negative voltage of approximately −0.6 V, thus limiting the reduction in array output power. Besides the power degradation, the shaded cells drastically change the overall *I–V* curve of PV module because of the bypass diodes. For this reason, several local MPP can form on the power–voltage (*P–V*) curve of a PV module/array. This causes serious problem in MPP tracking control of the system. Therefore, before the evaluation behavior of partially shaded PV arrays, bypass diodes must be included in PV module model.

The characteristic of *I–V* curve is also dependent on how the modules are shaded (Quaschning and Hanitsch, 1996). To be able to get the relationship between MPP of a module and the number of shaded cells and their irradiance level, a computer algorithm is developed. This algorithm allows analyzing PV module with down to the solar cell level. The number of series connected solar cell and the number of solar cells per one bypass diode in a module are the inputs of this algorithm. This feature facilitates using of the presented algorithm. The required equations for determining all the sub-voltages and sub-currents are obtained by using the Kirchhoff's current and voltage law for a given load voltage (V_{load}) at the output of PV array. We received inspiration from Quaschning and Hanitsch (1996) model for this algorithm. The cell-based algorithm for a single PV module is presented in the following equations (Eqs. (6)–(13)).

If c is the number of total solar cells in a single PV module and p is the number of solar cells per one bypass diode, the number of bypass diodes is expressed as

$$d = c/p \tag{6}$$

To be able to follow this algorithm easily, all the sub-voltages and currents are shown in Fig. 6 where the bypass diodes are shown connected over two solar cells, namely p here is equal to 2. The load voltage can be included by the following equation:

$$\sum_{i=1}^{c} V_i - V_{\text{load}} = 0 \tag{7}$$

For a single PV module with d bypass diodes, the mesh equations can be written as

$$\sum_{t=p\cdot(i-1)+1}^{i\cdot p} V_t + V_{c+d-1+i} = 0 \quad \text{for } i = 1, 2, \ldots, (d-1), d \tag{8}$$

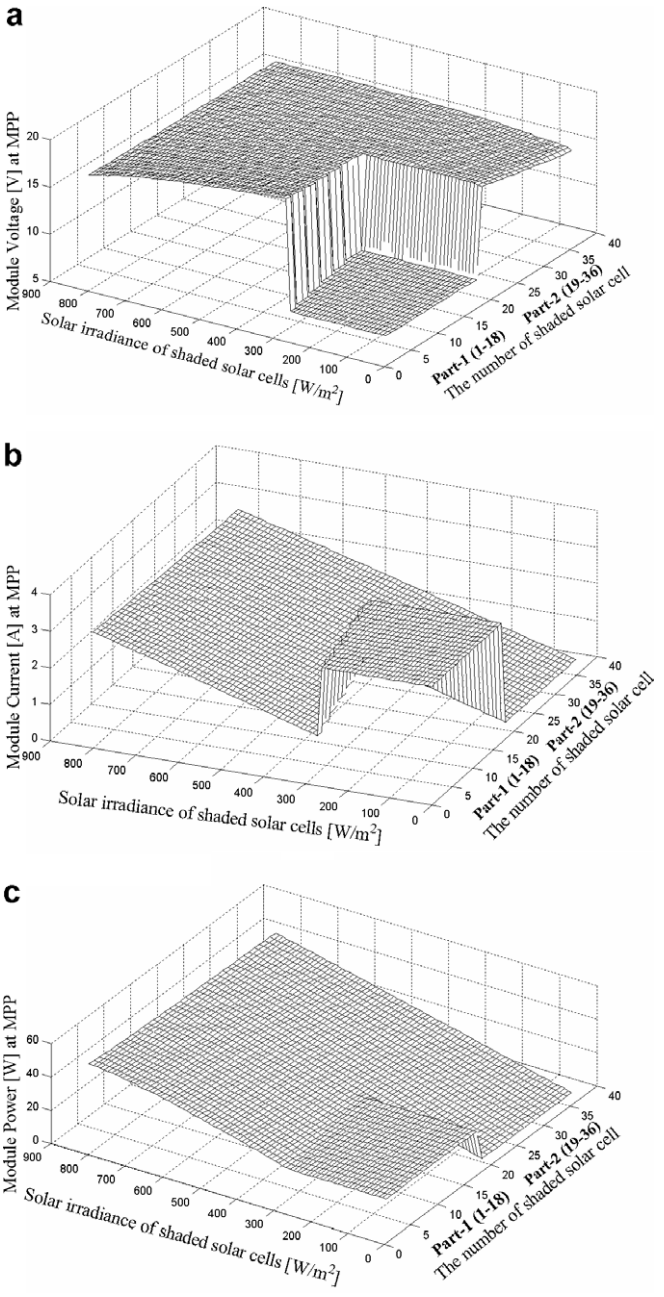

Fig. 7. The variation of the voltage (a), current (b) and power (c) of the SM 55 PV module at MPP as a parameter of the number of shaded solar cells and different shading level. (Irradiances of unshaded cells are 1000 W/m^2.)

The currents of series connected cells are the same. This relationship is given as

$$\begin{aligned} &\text{for } j = 1, \ldots, d \\ &I_n - I_{n+1} = 0 \quad \text{for } n = (p \cdot (j-1) + 1), \\ &\quad (p \cdot (j-1) + 1) + 1, \ldots, (j \cdot p - 1) \end{aligned} \tag{9}$$

According to Kirchhoff's currents law, the relationship of currents at junctions where the bypass diodes are connected is given as

$$I_{p \cdot i} - I_{p \cdot i+1} + I_{c+i} = 0 \quad \text{for } i = 1, \ldots, d-1 \tag{10}$$

$$I_{c+(d-1)+i} - I_{c+i} - I_{c+(d-1)+i+1} = 0 \quad \text{for } i = 1, \ldots, d-1 \tag{11}$$

For a single solar cell, the relationship between cell current and cell voltage is

$$\begin{aligned} &-I_i + I_{\text{ph}}(i) - I_{\text{s}}(i)\left[\exp\left[\frac{q\left[V_i + I_i R_{\text{s}}^{\text{cell}}(i)\right]}{n(i)kT(i)}\right] - 1\right] \\ &- \frac{V_i + I_i R_{\text{s}}^{\text{cell}}(i)}{R_{\text{p}}^{\text{cell}}(i)} = 0 \quad \text{for } i = 1, \ldots, c \end{aligned} \tag{12}$$

Because of using bypass diodes, it is not necessary to include the extension term given in Quaschning and Hanitsch (1996) for the negative diode breakdown. This extension term appears during avalanche breakdown at high negative voltages.

The terminal equations of bypass diodes can be written as follows:

$$\begin{aligned} &-I_{c+(d-1)+i} + I_{\text{sbd}}\left[\exp\left[\frac{q\left[V_{c+(d-1)+i}\right]}{n_{\text{bd}}kT_{\text{bd}}}\right] - 1\right] = 0 \\ &\text{for } i = 1, \ldots, d \end{aligned} \tag{13}$$

where I_{sbd}, n_{bd} and T_{bd} are bypass diode's saturation current, ideality factor and temperature, respectively. The following values are used in the simulation for bypass diodes: $I_{\text{sbd}} = 1.6 \times 10^{-9}$, $n_{\text{bd}} = 1$, and $T_{\text{bd}} = 35$ °C.

SM 55 PV module consists of 36 solar cells, and 18 cells are equipped with one bypass diode. So there are in total 39 unknown. When we determine the unknowns, the trust region method (McCartin, 1998) is used for solving the 39 couple equations that are given in Eqs. (6)–(13). The initial sub-voltages and sub-currents are taken as $V_{\text{load}}/36$ and zeros, respectively. All equivalent circuit parameters for each solar cell are updated by using the ANN for each operating condition. Since ANN structure is trained for a single PV module, only the series and parallel resistance values should be divided by 36 for a single solar cell (Gow and Manning, 1999).

The relationship of the MPP with the number of shaded cells and the irradiance of shaded cells are given in Fig. 7 for SM 55 PV module. It is assumed that the irradiance of unshaded cells is 1000 W/m^2 for all simulations. The irradiance of shaded solar cells is changed from 100 W/m^2 to 900 W/m^2 in sequence and the cell temperature is assumed as 35 °C. When a PV module that is equipped with two bypass diodes has one or more shaded cells, two peaks appear on the P–V curve. If the irradiance of shaded cells is greater than about 410 W/m^2, the second peak point, that has bigger voltage than the other peak point, is always global MPP. If the irradiance of shaded cell is smaller than about 370 W/m^2, the number of shaded cells determines which peak is global MPP. If shaded cells belong to the same bypass diode, the first peak is global MPP and the number of shaded cells does not affect the location of MPP significantly. Thus the PV module can be divided into two parts as shown in Fig. 7. If both the parts have one or more shaded cells, whose irradiation level

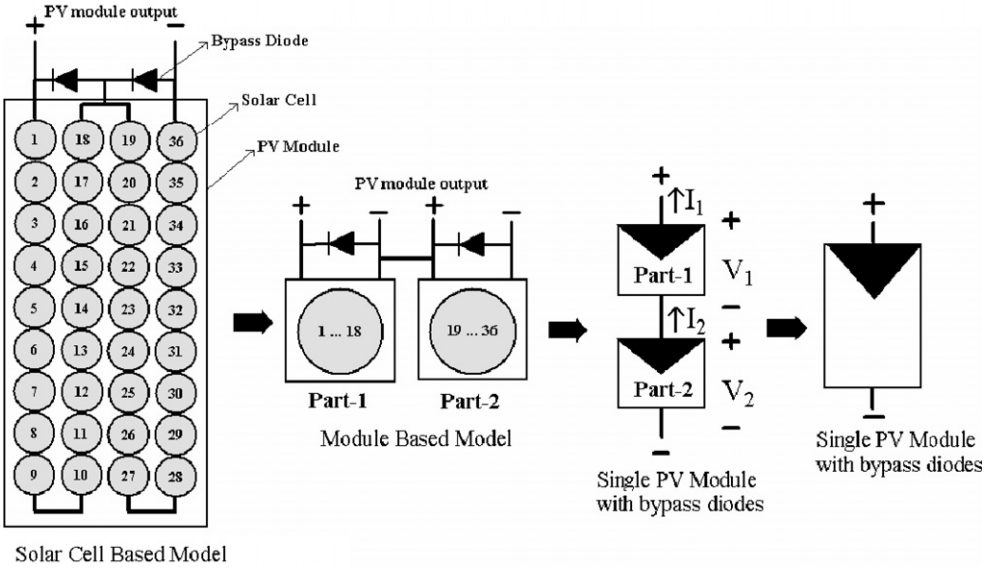

Fig. 8. Connection schematic of the solar cell and bypass diodes in the PV module.

is smaller than about 370 W/m^2, the second peak is always global MPP. The MPP is more dependent on shading level than the number of shaded cells. As can be seen in Fig. 7, if the cells where are in the both parts are shaded at the same time with an irradiance that is lower than about 370 W/m^2, the module power losses drastically increase. In this respect, to reduce the numerical computation time and effort in analyzing PV array characteristics, single PV module can be modeled as two modules that consist of 18 cells. To be able to compare the solar cell-based model with the module-based model, the second algorithm is written for SM 55 PV module.

In the second algorithm, single PV module is divided into two parts as shown in Fig. 8 and each part behaves

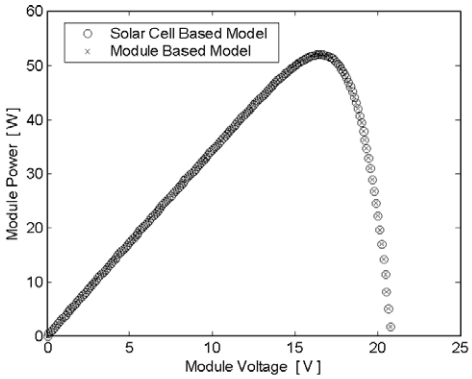

(a) Without mismatching (G = 1000 W/m^2, T=35°C).

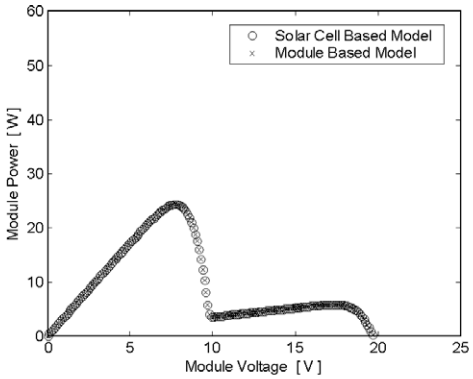

(b) For the cell-based model: from the 1st cell to the 18th cell: 100 W/m^2, for the module-based model: Part-1: 100 W/m^2.

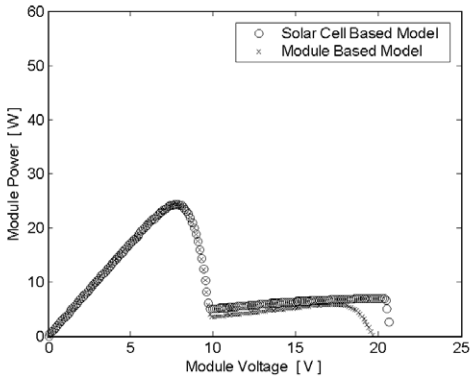

(c) For the cell-based model: the 1st cell: 100 W/m^2, for the module-based model: Part-1: 100 W/m^2.

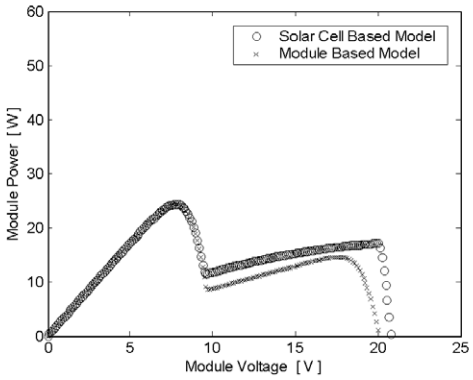

(d) For the cell-based model: the 1st cell: 250 W/m^2, for the module-based model: Part-1:250 W/m^2.

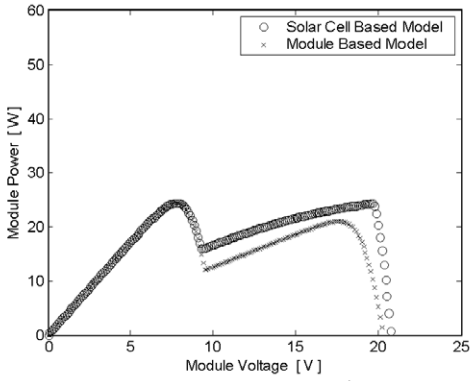

(e) For the cell-based model: the 1st cell: 360 W/m^2, for the module-based model: Part-1: 360 W/m^2.

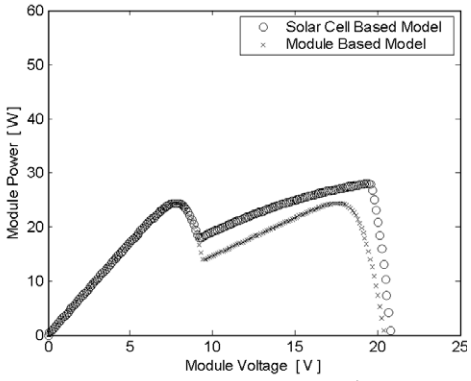

(f) For the cell-based model: the 1st cell: 420 W/m^2, for the module-based model: Part-1: 420 W/m^2.

Fig. 9. Power–voltage (*P–V*) characteristics as a parameter of different partially shading conditions for the solar cell-based and the module-based model.

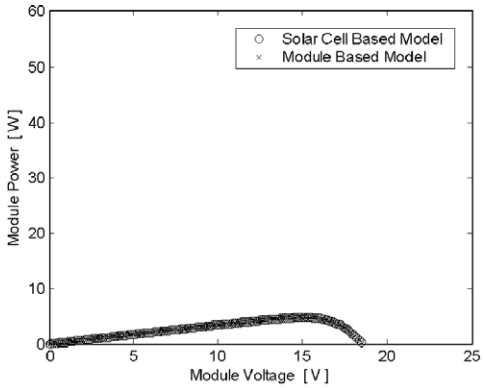

(g) For the cell-based model: from the 1st cell to the 36th cell: 100 W/m^2, for the module-based model: Part-1 and Part-2: 100 W/m^2.

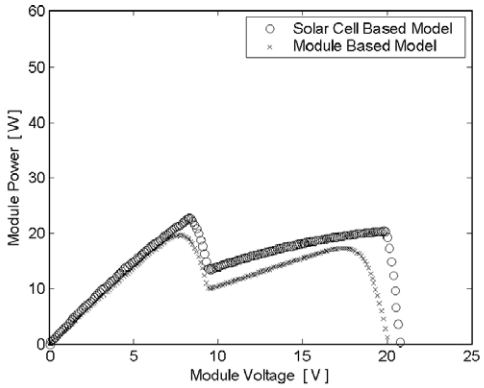

(h) For the cell-based model: the 1st cell: 300 W/m^2 and 19th cell: 800 W/m^2, for the module-based model: Part-1: 300 W/m^2 and Part-2: 800 W/m^2.

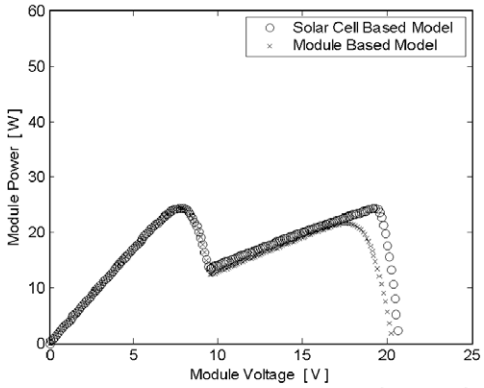

(i) For the cell-based model: the 1st, 2nd and 3rd cell: 370 W/m^2, for the module-based model: Part-1: 370 W/m^2.

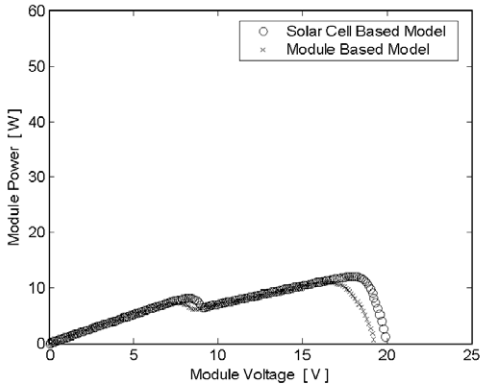

(j) For the cell-based model: from the 1st cell to the 5th cell: 200 W/m^2 and from the 19th cell to the 23rd cell: 300 W/m^2, for the module-based model: Part-1: 200 W/m^2 and Part-2: 300 W/m^2.

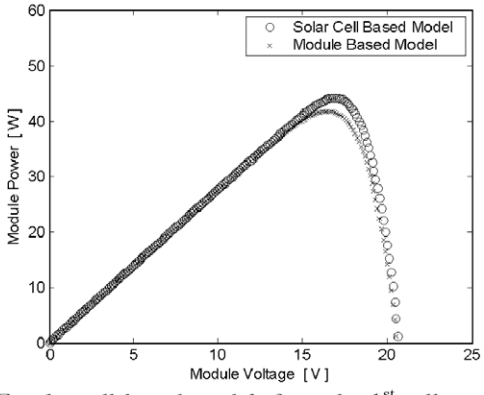

(k) For the cell-based model: from the 1st cell to the 10th cell and from the 19th cell to the 27th cell: 800 W/m^2, for the module-based model: Part-1 and Part-2: 800 W/m^2.

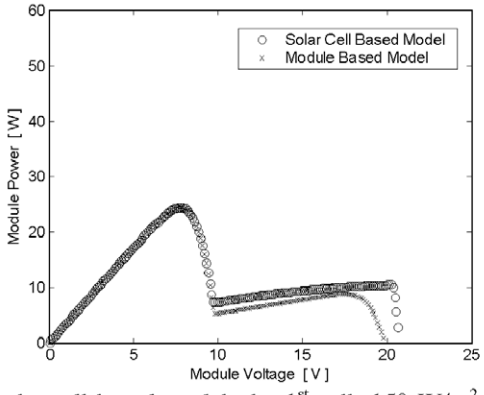

(l) For the cell-based model: the 1st cell: 150 W/m^2 and 5th cell: 750 W/m^2, for the module-based model: Part-1 150 W/m^2.

Fig. 9 (*continued*)

as a single module. The series and parallel resistances of each part are taken as half of the value of that determined by ANN mentioned in Section 2 (Gow and Manning, 1999). In this approach, the *I–V* equation of the bypass diode and PV module are combined into single equation (Eq. (14)), so this helps to reduce the numerical computation effort too. Equations of this model are constructed simply by using

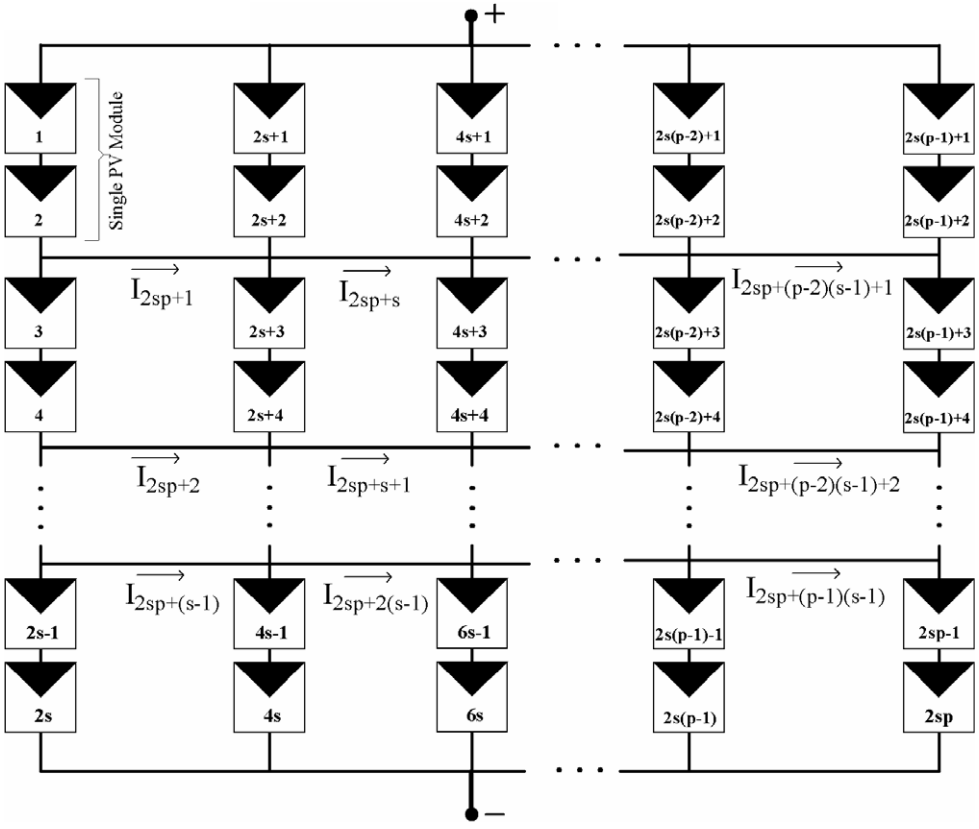

Fig. 10. General model for interconnection of PV arrays.

for $i = 1, 2$

$$-I_i + I_{\mathrm{ph}}(i) - I_{\mathrm{s}}(i)\left[\exp\left[\frac{q[V_i + I_i R_{\mathrm{s}}(i)]}{18n(i)kT(i)}\right] - 1\right] - \frac{V_i + I_i R_{\mathrm{s}}(i)}{R_{\mathrm{p}}(i)} + I_{\mathrm{sbd}}\left[\exp\left[-\frac{q[V_i]}{n_{\mathrm{bd}}kT_{\mathrm{bd}}}\right] - 1\right] = 0 \quad (14)$$

$$V_1 + V_2 - V_{\mathrm{load}} = 0 \quad (15)$$

$$I_1 - I_2 = 0 \quad (16)$$

where 1 and 2 indices represent Part-1 and Part-2, respectively (see Fig. 8).

Consequently, there are only four unknown in this case for a single module to get the I–V characteristic. This approach makes it easy to construct the large-scale PV array simulation algorithm and reduces the complexity. These two models are compared for different shading cases and the simulation results are shown in Fig. 9. From these figures, it can be seen that an almost good fit is obtained.

4. Current–voltage characteristics of PV arrays

There are considerable efforts for simulating the electrical behavior of partially shaded PV array and minimizing the mismatch losses through using different interconnection of PV modules (Woyte et al., 2003; Kaushika and Gautam, 2003; Ho and Wenham, 2001). In this paper, the proposed module-based model approach is used to simulate the PV arrays characteristics.

The 12 different array configurations are investigated here and they are shown in Fig. 11. All of them contain 12 Siemens SM 55 modules. The simulations of all PV arrays are merged in a new single algorithm. When the different interconnected PV arrays are analyzed, only the connection type and the size of the PV array are required as inputs for this algorithm. The general model for a PV array is given in Fig. 10 to follow the notation of voltages and currents easily. The required equations are formed by using Kirchhoff's laws and these are given by Eqs. (17)–(27). In the equations, s is the number of the module in a column and r is the number of the module in a row for a PV array.

In this algorithm, the load voltage of PV array can be included as

$$\sum_{i=1}^{2s} V_i - V_{\mathrm{load}} = 0 \quad (17)$$

The currents of Part-1 and Part-2 of each module must be equal:

$$I_{(j-1)2s+i} - I_{(j-1)2s+i+1} = 0 \quad \text{for } i = 1, 3, 5, \ldots, 2s-1; \quad \text{for } j = 1, 2, 3, \ldots, r \quad (18)$$

The sum of the currents in each node equals zero:

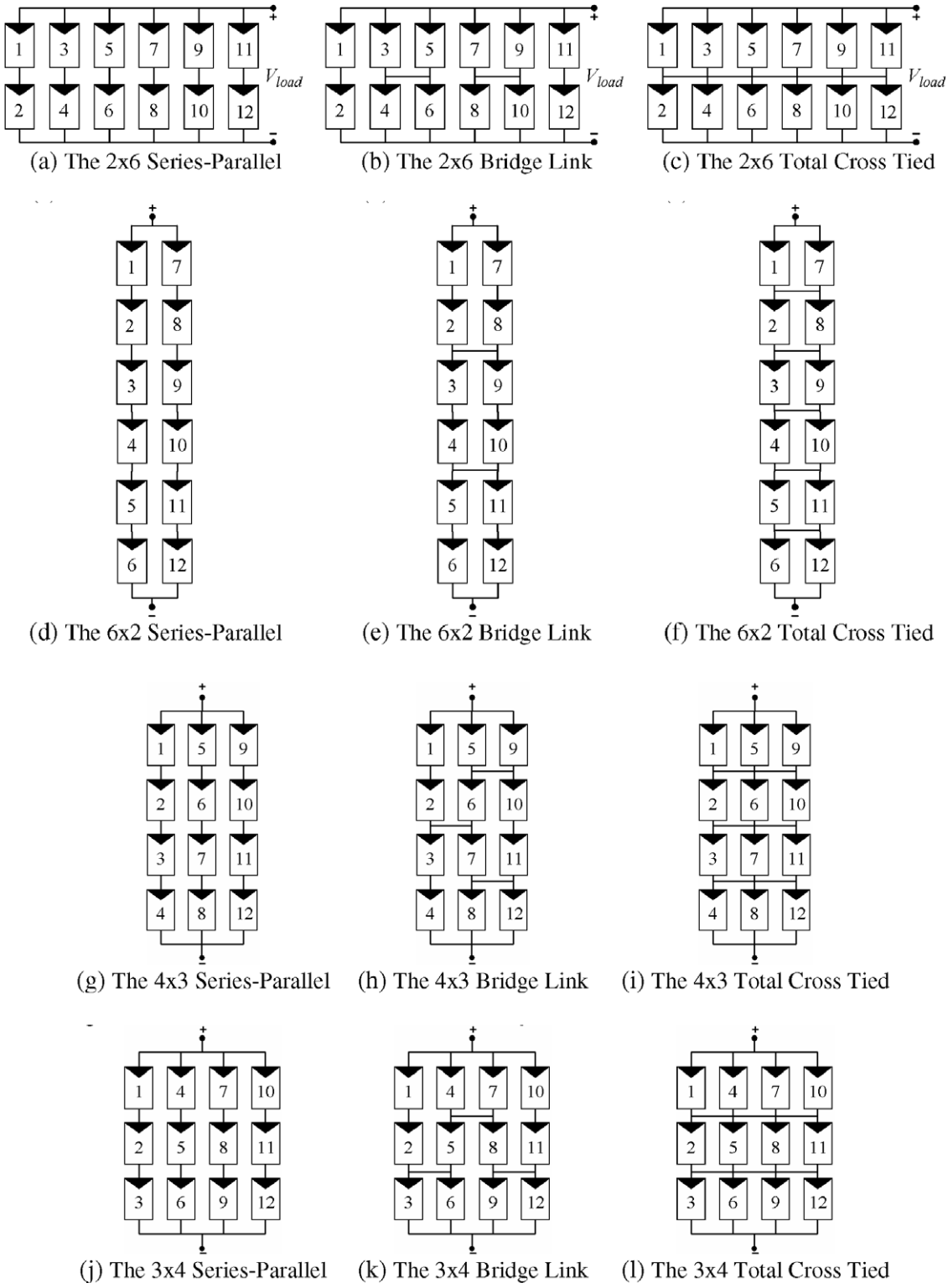

Fig. 11. Schematic diagram of PV array configurations.

$$I_{(j-1)2s+i} + I_{2sr+(j-1)(s-1)+i/2} - I_{(j-1)2s+i+1} - I_{2sr+(j-1)(s-1)+i/2-(s-1)} = 0$$
$$\text{for } i = 2,4,6,\ldots,2s-2; \quad \text{for } j = 1,2,3,\ldots,r \qquad (19)$$
$$\text{with } I_{2sr+(j-1)(s-1)+i/2-(s-1)} = 0 \quad \text{if } j = 1 \quad \text{and}$$
$$I_{2sr+(j-1)(s-1)+i/2} = 0 \quad \text{if } j = r$$

The sum of the voltages in each mesh equals zero:

$$V_{(j-1)2s+i-1} + V_{(j-1)2s+i} - V_{j2s+i-1} - V_{j2s+i} + V_{2sr+(j-1)(s-1)+i/2} - V_{2sr+(j-1)(s-1)+i/2-1} = 0$$
$$\text{for } i = 2,4,6,\ldots,2s; \quad \text{for } j = 1,2,3,\ldots,r-1$$

Table 3
Mismatch test conditions

Test set	The irradiances [W/m^2] of the Part-1 (P-1) and Part-2 (P-2) of the 12 PV modules																							
	Module-1		Module-2		Module-3		Module-4		Module-5		Module-6		Module-7		Module-8		Module-9		Module-10		Module-11		Module-12	
	P-1	P-2	P-1	P-2	P-1	P-2	P-1	P-2	P-1	P-2	P-1	P-2	P-1	P-2	P-1	P-2	P-1	P-2	P-1	P-2	P-1	P-2	P-1	P-2
1	1000	1000	1000	1000	1000	1000	1000	1000	1000	1000	1000	1000	1000	1000	1000	1000	1000	1000	1000	1000	1000	1000	1000	1000
2	755	767	898	371	316	103	111	406	523	984	106	288	582	427	450	654	984	388	567	670	168	956	832	552
3	167	118	243	367	229	148	143	220	101	328	150	208	136	109	237	241	338	362	247	345	348	258	328	111
4	884	509	756	766	406	579	709	791	792	806	559	458	595	540	776	838	959	794	528	978	752	950	842	996
5	112	975	963	972	971	993	968	974	967	989	983	981	956	1000	970	971	998	960	956	976	953	992	962	958
6	110	117	101	116	107	111	118	118	684	537	978	265	154	141	154	146	492	485	622	706	513	325	555	737
7	906	697	917	944	983	726	992	954	613	637	641	724	771	827	815	985	770	800	835	981	948	966	845	702
8	108	105	104	101	109	105	109	107	921	761	843	730	120	115	109	103	108	104	109	118	118	105	108	102
9	147	136	179	104	102	123	166	196	125	207	307	171	442	194	206	123	121	197	102	134	163	193	153	118
10	110	864	981	686	109	909	672	810	941	973	951	915	973	923	915	931	928	964	904	945	910	978	974	959
11	565	340	747	264	324	373	688	460	664	717	830	840	906	871	681	909	1000	941	907	225	243	242	409	234
12	940	530	971	674	805	529	598	517	482	490	392	541	617	956	981	784	580	940	300	613	785	994	923	475
13	237	375	295	277	207	740	418	254	962	718	631	295	933	316	855	512	106	449	423	122	102	108	132	433
14	566	799	828	987	402	952	950	867	901	629	255	383	460	537	707	957	215	796	472	381	895	970	864	892
15	415	347	218	236	323	392	332	288	363	343	325	381	451	420	417	408	748	365	598	688	244	727	769	886
16	627	652	575	582	842	855	810	788	630	854	838	540	613	617	661	638	567	569	555	570	664	610	720	764
17	607	458	377	377	535	697	577	440	569	330	393	534	538	585	436	327	632	670	621	626	842	803	823	896
18	377	387	406	383	757	758	300	319	729	767	741	781	302	321	880	866	866	861	855	867	645	573	647	691
19	672	675	178	132	763	793	164	174	784	699	706	682	671	651	153	189	703	710	701	720	676	657	666	669
20	182	802	806	801	247	801	316	484	192	889	837	451	809	836	804	891	892	854	889	860	871	872	812	820
21	101	470	527	496	124	591	219	132	142	521	518	520	509	506	553	420	527	493	442	606	602	451	448	615
22	708	540	744	841	501	588	628	844	504	577	798	989	771	511	544	941	869	848	511	715	610	913	853	843
23	100	100	1000	1000	1000	1000	1000	1000	1000	1000	1000	1000	1000	1000	1000	1000	1000	1000	1000	1000	1000	1000	1000	1000
24	200	200	1000	1000	1000	1000	1000	1000	1000	1000	1000	1000	1000	1000	1000	1000	1000	1000	1000	1000	1000	1000	1000	1000
25	300	300	1000	1000	1000	1000	1000	1000	1000	1000	1000	1000	1000	1000	1000	1000	1000	1000	1000	1000	1000	1000	1000	1000
26	400	400	1000	1000	1000	1000	1000	1000	1000	1000	1000	1000	1000	1000	1000	1000	1000	1000	1000	1000	1000	1000	1000	1000
27	500	500	1000	1000	1000	1000	1000	1000	1000	1000	1000	1000	1000	1000	1000	1000	1000	1000	1000	1000	1000	1000	1000	1000
28	600	600	1000	1000	1000	1000	1000	1000	1000	1000	1000	1000	1000	1000	1000	1000	1000	1000	1000	1000	1000	1000	1000	1000
29	700	700	1000	1000	1000	1000	1000	1000	1000	1000	1000	1000	1000	1000	1000	1000	1000	1000	1000	1000	1000	1000	1000	1000
30	800	800	1000	1000	1000	1000	1000	1000	1000	1000	1000	1000	1000	1000	1000	1000	1000	1000	1000	1000	1000	1000	1000	1000

Table 4
The maximum power points of PV array configurations for the mismatch test conditions

Test set	PV array configurations																	
	2 × 6 – SP			2 × 6 – BL			2 × 6 – TCT			6 × 2 – SP			6 × 2 – BL			6 × 2 – TCT		
	P_{mp} [W]	V_{mp} [V]	I_{mp} [A]	P_{mp} [W]	V_{mp} [V]	I_{mp} [A]	P_{mp} [W]	V_{mp} [V]	I_{mp} [A]	P_{mp} [W]	V_{mp} [V]	I_{mp} [A]	P_{mp} [W]	V_{mp} [V]	I_{mp} [A]	P_{mp} [W]	V_{mp} [V]	I_{mp} [A]
1	589.79	31.17	18.91	589.79	31.17	18.91	589.79	31.17	18.91	589.79	93.52	6.30	589.79	93.52	6.30	589.79	93.52	6.30
2	215.42	24.32	8.85	227.82	23.87	9.54	234.50	32.50	7.21	190.04	75.61	2.51	210.73	64.34	3.27	205.87	92.20	2.23
3	91.21	23.21	3.92	101.76	22.55	4.51	109.69	30.73	3.56	90.98	70.31	1.29	83.97	71.63	1.17	87.24	71.63	1.21
4	354.68	33.16	10.69	379.05	32.50	11.66	401.68	32.06	12.52	327.50	102.81	3.18	360.36	100.82	3.57	366.50	90.21	4.06
5	490.18	31.39	15.61	498.72	31.61	15.77	516.13	31.83	16.21	540.72	88.22	6.12	525.19	86.23	6.09	525.19	86.23	6.09
6	153.36	24.54	6.24	152.29	24.10	6.31	173.98	30.95	5.62	109.20	54.39	2.01	109.61	55.05	1.99	127.81	63.67	2.01
7	457.55	32.50	14.07	463.35	32.28	14.35	473.99	31.83	14.88	442.77	98.83	4.48	450.17	98.83	4.55	452.54	98.83	4.57
8	121.50	29.84	4.07	121.69	29.84	4.07	122.19	29.84	4.09	77.27	27.85	2.77	75.52	27.85	2.71	74.05	27.19	2.72
9	70.16	30.95	2.26	76.79	30.73	2.49	79.29	30.29	2.61	66.31	95.51	0.69	71.04	94.19	0.75	71.68	94.19	0.76
10	421.55	25.64	16.43	423.34	25.64	16.50	421.70	32.28	13.06	446.76	84.24	5.30	427.89	81.58	5.24	425.06	80.92	5.25
11	263.82	23.65	11.15	276.11	32.28	8.55	292.04	32.72	8.92	235.72	55.71	4.23	275.01	89.54	3.07	278.70	90.87	3.06
12	313.03	33.16	9.43	320.37	32.94	9.72	344.11	32.72	10.51	304.01	84.24	3.61	307.41	82.91	3.70	308.10	81.58	3.77
13	151.58	24.54	6.17	158.84	32.72	4.85	169.95	32.06	5.30	125.17	47.09	2.65	138.33	56.38	2.45	167.07	63.01	2.65
14	303.17	24.10	12.57	330.23	32.72	10.09	346.69	32.72	10.59	273.72	54.39	5.03	314.10	91.53	3.43	322.51	92.20	3.49
15	205.54	24.10	8.52	208.02	23.65	8.79	220.24	32.28	6.82	189.83	80.26	2.36	185.85	93.52	1.98	198.31	99.49	1.99
16	380.14	31.61	12.02	384.38	31.61	12.15	387.26	31.39	12.33	358.39	98.17	3.65	369.86	96.18	3.84	382.88	94.85	4.03
17	303.34	32.06	9.46	309.78	32.06	9.66	314.28	31.83	9.87	257.39	82.91	3.10	260.01	80.92	3.21	270.83	80.26	3.37
18	322.07	31.61	10.18	331.92	32.06	10.35	366.53	31.17	11.75	267.61	82.91	3.22	256.20	63.01	4.06	310.83	79.59	3.90
19	253.56	31.61	8.01	257.60	32.06	8.03	271.25	32.50	8.34	276.38	63.67	4.34	267.74	61.68	4.34	262.97	61.02	4.30
20	330.63	25.20	13.11	328.53	24.76	13.26	338.43	32.50	10.41	317.82	88.88	3.57	323.10	96.84	3.33	331.51	98.83	3.35
21	193.98	23.21	8.35	194.75	24.10	8.08	196.59	32.50	6.04	176.78	95.51	1.85	182.01	98.17	1.85	191.13	98.17	1.94
22	353.67	33.16	10.66	368.97	32.72	11.27	380.30	32.50	11.70	344.51	100.82	3.41	346.53	100.16	3.45	359.64	100.16	3.59
23	502.09	31.17	16.10	510.30	31.61	16.13	527.38	31.61	16.67	511.58	81.58	6.27	484.87	76.94	6.30	484.87	76.94	6.30
24	512.79	31.39	16.33	520.74	31.61	16.47	535.92	31.61	16.95	511.62	81.58	6.27	484.92	76.94	6.30	484.92	76.94	6.30
25	523.54	31.39	16.67	531.07	31.61	16.79	544.13	31.61	17.20	511.67	81.58	6.27	484.98	76.94	6.30	484.98	76.94	6.30
26	534.23	31.39	17.01	541.19	31.61	17.11	551.92	31.61	17.45	511.73	81.58	6.27	485.05	76.94	6.30	485.05	76.94	6.30
27	544.84	31.39	17.35	550.97	31.61	17.42	559.35	31.39	17.81	511.81	81.58	6.27	508.06	100.16	5.07	508.06	100.16	5.07
28	555.31	31.39	17.68	560.35	31.61	17.72	566.39	31.39	18.04	511.92	81.58	6.27	532.92	98.83	5.39	532.92	98.83	5.39
29	565.49	31.39	18.01	569.24	31.39	18.13	572.97	31.39	18.24	526.84	97.50	5.40	554.71	96.84	5.72	554.71	96.84	5.72
30	575.07	31.39	18.31	577.25	31.39	18.38	579.05	31.17	18.57	557.71	96.84	5.75	571.87	95.51	5.98	571.87	95.51	5.98
	3 × 4 – SP			3 × 4 – BL			3 × 4 – TCT			4 × 3 – SP			4 × 3 – BL			4 × 3 – TCT		
1	589.79	46.76	12.61	589.79	46.76	12.61	589.79	46.76	12.61	589.79	62.35	9.45	589.79	62.35	9.45	589.79	62.35	9.45
2	193.27	41.12	4.69	243.63	40.13	6.07	210.90	41.45	5.08	213.52	49.08	4.35	196.45	49.52	3.96	211.90	38.47	5.50
3	88.85	39.46	2.25	94.08	47.42	1.98	99.83	47.75	2.09	93.74	55.71	1.68	96.38	46.43	2.07	103.73	62.79	1.65
4	333.17	51.07	6.52	366.47	49.08	7.46	379.83	49.41	7.68	347.08	57.48	6.03	357.72	56.60	6.32	375.97	65.88	5.70
5	520.39	42.78	12.16	498.62	40.79	12.22	490.48	49.08	9.99	531.70	57.92	9.17	509.18	55.71	9.13	504.11	54.83	9.19
6	120.42	34.49	3.49	137.65	30.18	4.56	159.79	48.09	3.32	138.34	56.60	2.44	147.68	57.93	2.54	147.25	56.16	2.62
7	450.87	48.75	9.24	457.64	48.75	9.38	463.99	48.75	9.51	447.21	65.88	6.78	454.96	65.00	6.99	458.38	65.44	7.00
8	107.95	31.50	3.42	102.79	30.18	3.40	99.48	29.18	3.41	93.84	30.51	3.07	89.23	29.18	3.05	87.96	28.74	3.06
9	70.49	46.76	1.50	73.49	46.76	1.57	78.07	45.76	1.71	69.13	62.79	1.10	75.37	61.90	1.21	77.52	61.46	1.26
10	404.89	48.09	8.41	408.18	48.09	8.48	426.26	48.75	8.74	421.41	51.29	8.21	411.59	50.41	8.16	421.50	65.00	6.48

(*continued on next page*)

Table 4 (*continued*)

	3×4 – SP		3×4 – BL		3×4 – TCT		4×3 – SP		4×3 – BL		4×3 – TCT	
11	273.69	50.08	5.46	285.22	49.74	5.73	297.74	48.42	6.14	256.04	65.88	3.88	268.67	58.81	4.56	286.74	65.00	4.41
12	303.57	50.08	6.06	317.03	49.74	6.37	326.49	49.74	6.56	294.40	59.25	4.96	307.24	57.48	5.34	314.97	67.65	4.65
13	136.46	32.17	4.24	148.72	31.50	4.72	168.82	31.50	5.35	146.81	50.41	2.91	146.29	49.96	2.92	151.13	49.52	3.05
14	291.57	31.50	9.25	306.70	41.12	7.45	315.61	41.12	7.67	283.77	40.24	7.05	306.60	57.92	5.29	319.73	66.77	4.78
15	206.82	41.12	5.02	213.01	40.13	5.31	216.62	39.46	5.48	199.89	48.20	4.14	200.37	48.64	4.11	216.82	65.00	3.33
16	360.05	48.42	7.43	367.97	48.09	7.65	384.73	47.42	8.11	362.76	65.00	5.58	362.27	65.00	5.57	365.35	65.00	5.62
17	274.95	49.74	5.52	291.85	48.42	6.02	299.92	48.75	6.15	289.47	65.44	4.42	299.45	64.56	4.63	300.30	64.56	4.65
18	264.40	31.50	8.39	303.99	49.41	6.15	306.44	49.74	6.15	277.23	48.20	5.75	287.73	67.65	4.25	352.38	64.12	5.49
19	269.85	31.17	8.65	262.05	48.42	5.41	275.18	49.74	5.53	237.08	48.64	4.87	228.86	47.75	4.79	245.92	48.20	5.10
20	321.08	43.77	7.33	325.81	48.42	6.72	350.50	48.42	7.23	311.03	61.02	5.09	314.01	59.69	5.26	351.63	55.71	6.31
21	178.05	48.75	3.65	180.01	49.08	3.66	197.98	39.46	5.01	191.63	57.48	3.33	190.91	57.04	3.34	193.92	57.48	3.37
22	344.17	50.41	6.82	345.01	50.41	6.84	367.81	49.74	7.39	343.30	66.77	5.14	352.00	66.77	5.27	367.10	66.77	5.49
23	458.49	47.09	9.73	482.41	48.42	9.96	502.53	48.75	10.31	476.53	50.41	9.45	458.55	66.33	6.91	470.37	66.77	7.04
24	474.67	47.09	10.07	497.70	48.42	10.27	515.63	48.42	10.64	476.60	50.41	9.45	478.28	65.88	7.25	489.07	66.33	7.37
25	490.91	47.09	10.42	512.68	48.42	10.58	528.15	48.42	10.90	476.69	50.41	9.45	497.43	65.44	7.60	506.98	65.88	7.69
26	507.20	47.42	10.69	527.21	48.09	10.96	540.02	48.09	11.22	480.25	63.23	7.59	515.76	65.00	7.93	523.87	65.00	8.05
27	523.46	47.42	11.03	541.03	48.09	11.25	551.02	47.75	11.53	502.14	63.67	7.88	533.08	64.56	8.25	539.61	64.56	8.35
28	539.63	47.42	11.37	554.04	47.75	11.60	561.10	47.42	11.83	523.95	63.67	8.22	549.09	64.12	8.56	553.84	64.12	8.63
29	555.48	47.42	11.71	565.82	47.42	11.93	570.10	47.09	12.10	545.49	64.12	8.50	563.25	63.67	8.84	566.22	63.23	8.95
30	570.32	47.42	12.02	575.90	47.09	12.22	577.87	47.09	12.27	565.78	63.67	8.88	574.94	62.79	9.15	576.36	62.79	9.17

with $V_{2sr+(j-1)(s-1)+i/2-1} = 0$ if $i = 2$ and

$$V_{2sr+(j-1)(s-1)+i/2} = 0 \quad \text{if } i = 2s \tag{20}$$

For each module part, the relationship between the current and the voltage is given by the following equation:

$$-I_i + I_{\mathrm{ph}}(i) - I_{\mathrm{s}}(i)\left[\exp\left[\frac{q[V_i + I_i R_{\mathrm{s}}(i)]}{n(i)kT(i)}\right] - 1\right] - \frac{V_i + I_i R_{\mathrm{s}}(i)}{R_{\mathrm{p}}(i)} + \cdots I_{\mathrm{sbd}}\left[\exp\left[-\frac{q[V_i]}{n_{\mathrm{bd}}kT_{\mathrm{bd}}}\right] - 1\right] = 0 \quad \text{for } i = 1, 2, 3, \ldots, 2sr \tag{21}$$

If the connection type is series–parallel (SP):

$$I_{2sr+(j-1)(s-1)+i} = 0 \quad \text{for } i = 1, 2, 3, \ldots, (s-1); \quad \text{for } j = 1, 2, 3, \ldots r-1 \tag{22}$$

If the connection type is total cross tied (TCT):

$$V_{2sr+(j-1)(s-1)+i} = 0 \quad \text{for } i = 1, 2, 3, \ldots, (s-1); \quad j = 1, 2, 3, \ldots r-1 \tag{23}$$

If the connection type is bridge-linked (BL):

$$I_{2sr+(j-1)(s-1)+i} = 0 \quad \text{for } i = 1, 3, 5, \ldots, (s-1);\ j = 1, 3, 5, \ldots, r-1 \tag{24}$$

$$V_{2sr+(j-1)(s-1)+i} = 0 \quad \text{for } i = 1, 3, 5, \ldots, (s-1);\ j = 2, 4, 6, \ldots, r-1 \tag{25}$$

$$V_{2sr+(j-1)(s-1)+i} = 0 \quad \text{for } i = 2, 4, 6, \ldots, (s-1);\ j = 2, 4, 6, \ldots, r-1 \tag{26}$$

$$I_{2sr+(j-1)(s-1)+i} = 0 \quad \text{for } i = 2, 4, 6, \ldots, (s-1);\ j = 1, 3, 5, \ldots, r-1 \tag{27}$$

For each configuration, all sub-voltage and sub-currents can be determined by the solution of a system of $2sr + (s-1)(r-1)$ simultaneous nonlinear equations for different operating conditions. Various different mismatch conditions can be investigated to evaluate the I–V characteristics of PV arrays and the variations of their MPP. However, it is difficult to examine all conditions. To get reliable conclusions, 30 shading scenarios are generated randomly within different irradiance intervals and each part of the PV modules is operated with these conditions. There are 24 different irradiance values in each scenario since each PV module has 2 parts (see Figs. 8 and 11). Shading scenarios are given in Table 3. While generating random scenarios, it is noticed that parts 1 and 2 on each module are irradiated in a different way for each scenario. The temperature of both parts of modules is assumed as 45 °C. The global MPP of each configuration is investigated for the shading scenarios and the results are given in Table 4.

5. Results and discussion

The incident irradiation composed of diffuse and direct components in a PV array do not distribute homogeneously through modules due to the effects of clouds, fog,

Table 5
The comparison of PV array configurations for the mismatch test conditions

PV array configurations	The mean value of MPP power	The RMSD value of MPP power	The mean value of MPP voltage	The RMSD value of MPP voltage
2×6 – SP	355.10	287.65	29.18	4.15
2×6 – BL	362.17	281.58	30.01	3.60
2×6 – TCT	372.92	272.56	31.73	0.93
6×2 – SP	338.78	304.26	80.32	22.29
6×2 – BL	341.26	300.12	82.79	20.58
6×2 – TCT	347.25	293.05	84.59	18.42
3×4 – SP	340.83	299.14	43.92	7.25
3×4 – BL	352.55	289.17	45.54	5.92
3×4 – TCT	361.75	281.69	46.05	5.22
4×3 – SP	339.55	298.60	56.52	10.48
4×3 – BL	345.43	295.32	58.46	9.33
4×3 – TCT	355.68	285.97	60.51	9.13

haze, dust, trees, buildings, walls and other matter in the environment. One way to reduce such mismatch effects is to make sure that the system is sited in an area where shading is minimal. But it cannot overcome performance degradation completely. Different interconnection configurations are very effective way to reduce such effects. In this study, the capability of various interconnection schemes is analyzed in detail by taking into consideration module bypass diodes.

In the first stage of this study, the variation of the MPP voltage, current and power of single module as a parameter of the number of shaded solar cells and different shading levels are presented in Fig. 7. As shown in Figs. 7 and 9, when there are different irradiated cells in a single module, the minimum irradiated cell is the most effective on the variations of the power–voltage characteristic for PV module. It is not important which cells are shaded on condition that their shading levels are the same to determine global MPP. These results allow using the proposed module-based model to investigate the electrical behavior of PV module without increasing the computational effort. As described before, the variation of the equivalent series and parallel resistances of a partially shaded module are also included by using ANN easily. This reduces discrepancy between experimental and theoretical results for PV module under shadow conditions (Sharma et al., 1991).

The proposed model is used to analyze the I–V characteristic of the 12 different connected PV arrays. To get a compressive comparison, MPP of these configurations is investigated under the 30 different operating conditions. The performance index of each configuration for maximum output power and MPP voltage is determined by the root mean square deviation (RMSD) from the MPP, which is when the irradiance of all modules is 1000 W/m^2. In addition, the mean values of MPP powers and voltages for each configuration are given in Table 5.

Besides the maximum output power of the configurations, their MPP voltage has to be taken into consideration. Voltage based MPP tracking algorithm is the most commonly used method, which moves the operating point toward the MPP periodically increasing or decreasing the PV array voltage by comparing the power with that of the previous perturbation cycle. The operating point oscillates around the MPP giving rise to the wastege of some amount of available energy (Femia et al., 2005) and this method may not detect the global MPP under some operating conditions. In this respect, 2×6 – TCT configuration gives the best results as shown in Table 5. We can conclude that the number of series connected modules should be decreased for reducing mismatch losses in a PV array and the TCT arrays show better performance for MPP powers and voltages. However, in Kaushika and Gautam (2003), it was shown that BL arrays give a better fault-tolerance in maximum output power in the partially shading cases. The underlying difference between their and our result may be due to the following reasons. In their study, the variations of the equivalent circuit parameters with respect to operating conditions were not included and bypass diodes effects were not considered. In our study, furthermore it is shown that TCT arrays have the minimum oscillation at MPP point. These results can also contribute to develop the MPP tracking of PV systems in a simple manner.

6. Conclusions

In this paper, we have investigated interconnected PV arrays by using a proposed PV module model. The equivalent circuit parameters of different irradiated PV modules in a PV array are estimated by using the ANN and this model is found useful to characterize the partially shaded PV module. It is proven that partially shading effects change the MPP of PV arrays. The bypass diodes should be included to investigate the influence of the mismatching effects in the power–voltage characteristic of a PV array. When the electrical characteristics of interconnected PV array networks are investigated, besides the maximum output power, the variation interval of the MPP voltage should be taken into consideration since the window of MPP tracking voltage of the dc/dc and dc/ac power converters is restricted. The results show that the superiority of the TCT configuration is clear in both respects.

References

Araki, K., Yamaguchi, M., 2003. Novel equivalent circuit model and statistical analysis in parameters identification. Solar Energy Materials and Solar Cells 75, 457–466.

Blas, M.A., Torres, J.L., Prieto, E., Garcia, A., 2002. Selecting a suitable model for characterizing photovoltaic devices. Renewable Energy 25, 371–380.

Ding, J., Cheng, X., Fu, T., 2005. Analysis of series resistance and *P–T* characteristics of the solar cell. Vacuum 77, 163–167.

Duffie, J.A., Beckman, W.A., 1991. Solar Engineering and Thermal Processes. John Wiley & Sons Inc., New York.

Dyk, E.E.V., Meyer, E.L., 2004. Analysis of the effect of parasitic resistance on the performance of photovoltaic modules. Renewable Energy 29, 333–334.

Dyk, E.E.V., Meyer, E.L., Vorster, F.J., Leitch, A.W.R., 2002. Long-term monitoring of photovoltaic devices. Renewable Energy 25, 183–197.

El-Adawi, M.K., Al-Nuaim, I.A., 2002. A method to determine the solar cells series resistance from a single *I–V*. Characteristic curve considering its shunt resistance – new approach. Vacuum 64, 33–36.

Femia, N., Petrone, G., Spagnuolo, Vitelli, M., 2005. Optimization of Perturb and observe maximum power point tracking method. IEEE Transactions on Power Electronics 20 (4), 963–973.

Gow, J.A., Manning, C.D., 1999. Development of photovoltaic array model for use in power-electronics simulation studies. IEE Proceedings of the Electrical Power Appliances 146 (2), 193–200.

Ho, A.W.Y., Wenham, S.R., 2001. Intelligent strategies for minimizing mismatch losses in photovoltaic modules and systems. 17th European Photovoltaic Solar Energy Conference and Exhibition, Munich-Germany.

Ikegami, T., Maezono, T., Nakanishi, F., Yamagata, Y., Ebihara, K., 2001. Estimation of equivalent circuit parameters of PV module and its application to optimal operation of PV system. Solar Energy Materials and Solar Cells 67, 389–395.

Kalman, B., Kwasny, S.C., 1992. Why tanh: choosing a sigmoidal function. IEEE International Joint Conference on Neural Network 4, 578–581.

Karatepe, E., Boztepe, M., Colak, M., 2006. Neural network based solar cell model. Energy Conversion and Management 47, 1159–1178.

Kaushika, N.D., Gautam, N.K., 2003. Energy yield simulations of interconnected solar PV arrays. IEEE Transactions on Energy Conversion 18 (1), 127–134.

Kawamura, H., Naka, K., et al., 2003. Simulation of *I–V* characteristics of a PV module with shaded PV cells. Solar Energy Materials and Solar Cells 75, 613–621.

King, D.L., (Version, 2000). Sandia's PV Module Electrical Performance Model. Sandia National Laboratories, Albuquerque, New Mexico, September 5.

Lu, L., Yang, H.X., 2004. A study on simulations of the power output and practical models for building systems. Journal of Solar Energy Engineering 126, 929–935.

McCartin, B.J., 1998. A model-trust region algorithm utilizing a quadratic interpolate. Journal of Computational and Applied Mathematics 91, 249–259.

Merten, J., Asensi, J.M., Voz, C., Shah, A.V., Platz, R., Andreu, J., 1998. Improved equivalent circuit and analytical model for amorphous silicon solar cells and modules. IEEE Transactions on Electron Devices 45 (2), 423–429.

Meyer, E.L., Dyk, E.E.V., 2004. Assessing the reliability and degradation of photovoltaic module performance parameters. IEEE Transactions on Reliability 53 (1), 83–92.

Oozeki, T., Izawa, T., Otani, K., Kurokawa, K., 2003. An evaluation method of PV systems. Solar Energy Materials and Solar Cells 75, 687–695.

Quaschning, V., Hanitsch, R., 1996. Numerical simulation of current–voltage characteristics of photovoltaic systems with shaded solar cells. Solar Energy 56, 513–520.

Reed, R., 1993. Pruning algorithms – a survey. IEEE Transactions on Neural Networks 4 (5), 740–747.

Scales, L.E., 1985. Introduction to Non-Linear Optimization. Springer-Verlag, Inc.

Sharma, A.K., Dwivedi, R., Srivastava, S.K., 1991. Performance analysis of a solar array under shadow condition. IEE Proceedings-G 138 (3), 301–306.

Teng, K.F., Wu, P., 1989. PV module characterization using Q-R decomposition based on the least square method. IEEE Transactions on Industrial Electronics 36 (1), 71–75.

Virtuani, A., Lotter, E., Powalla, M., 2003. Performance of Cu(In,Ga)Se_2 solar cells under low irradiance. Thin Solid Films, 431–432, 443–447.

Weinstock, D., Appelbaum, J., 2004. Shadow Variation on Photovoltaic Collectors in a Solar Field. 23rd IEEE Convention of Electrical and Electronics Engineers, pp. 354–357.

Woyte, A., Nijs, J., Belmans, R., 2003. Partial shadowing of photovoltaic arrays with different system configurations: literature review and field test results. Solar Energy 74, 217–233.

Zurada, J.M., 1992. Introduction to Artificial Neural Systems. West Publishing Company.